6-7-2019

The foot and ankle structures reveal emergent properties analogous to passive springs during human walking

Erica Hedrick
University of Nebraska at Omaha, ehedrick@unomaha.edu

Steven J. Stanhope
University of Delaware

Kota Z. Takahashi
University of Nebraska at Omaha, ktakahashi@unomaha.edu

Recommended Citation
Hedrick EA, Stanhope SJ, Takahashi KZ (2019) The foot and ankle structures reveal emergent properties analogous to passive springs during human walking. PLoS ONE 14(6): e0218047. https://doi.org/10.1371/journal.pone.0218047

PLOS ONE

The foot and ankle structures reveal emergent properties analogous to passive springs during human walking

Erica A. Hedrick , Steven J. Stanhope, Kota Z. Takahashi

Published: June 7, 2019 • https://doi.org/10.1371/journal.pone.0218047

Abstract

An objective understanding of human foot and ankle function can drive innovations of bio-inspired wearable devices. Specifically, knowledge regarding how mechanical force and work are produced within the human foot-ankle structures can help determine what type of materials or components are required to engineer devices. In this study, we characterized the combined functions of the foot and ankle structures during walking by synthesizing the total force, displacement, and work profiles from structures distal to the shank. Eleven healthy adults walked at four scaled speeds. We quantified the ground reaction force and center-of-pressure displacement in the shank's coordinate system during stance phase and the total mechanical work done by these structures. This comprehensive analysis revealed emergent properties of foot-ankle structures that are analogous to passive springs: these structures compressed and recoiled along the longitudinal axis of the shank, and performed near zero or negative net mechanical work across a range of walking speeds. Moreover, the subject-to-subject variability in peak force, total displacement, and work were well explained by three simple factors: body height, mass, and walking speed. We created a regression-based model of stance phase mechanics that can inform the design and customization of wearable devices that may have biomimetic or non-biomimetic structures.

Citation: Hedrick EA, Stanhope SJ, Takahashi KZ (2019) The foot and ankle structures reveal emergent properties analogous to passive springs during human walking. PLoS ONE 14(6): e0218047. https://doi.org/10.1371/journal.pone.0218047

Editor: John Leicester Williams, University of Memphis, UNITED STATES

Received: February 7, 2019; **Accepted:** May 24, 2019; **Published:** June 7, 2019

Data Availability: All relevant data are within the manuscript and its Supporting Information files.

Funding: This work was supported by funding from the Center for Research in Human Movement Variability of the University of Nebraska at Omaha and the National Institute of Health (P20GM109090) awarded to KT.

Competing interests: The authors have declared that no competing interests exist.

Introduction

An objective understanding of human foot and ankle function can help identify the mechanisms that underlie healthy locomotion, and drive innovations and development of bioinspired wearable devices, such as prostheses and exoskeletons. For example, knowledge of the mechanical forces and work in the human foot and ankle are informative for understanding how the anatomical structures change the body's energy states. Muscles in the lower limb such as the ankle plantarflexors do work through active muscles contractions [1–7]. Elastic structures such as the plantar fascia [8–11] and Achilles tendon [6, 7, 10, 12–16] can store and return mechanical energy [17]. Examining the work production of biological structures can determine what material characteristics (e.g., elastic or viscous) or components (e.g., battery-powered actuators) are needed for device designs to emulate natural structures and/or functions.

Bio-inspiration has been central to the recent development of ankle-related devices, such as exoskeletons and prostheses. The biological ankle structures, in particular the plantar flexor muscle-tendon structures, play an important role in providing body support, forward propulsion, and initiating swing [5, 13]. These structures produce the largest proportion of positive work during the stance phase of walking [2, 12, 18], utilizing elastic structures such as the Achilles tendon [6, 7, 10, 12–16], and active muscles [1–7]. As such, certain functions of the biological ankle have been emulated with unpowered and powered devices. For example, unpowered exoskeletons [19] or orthoses [20–22] designed with elastic materials can store energy through torsional stiffness at the ankle and provide push-off power via elastic energy return. Powered exoskeletons [23–27] and prostheses [28–30] emulate active plantarflexion by generating a burst of positive ankle power during late stance. These bio-inspired devices attempt to replicate how an isolated region (i.e., ankle joint) behaves in humans without necessarily precisely replicating the designs of these regions. However, this approach does not take into account the properties of more distal structures in the foot, which also exhibit unique energetic characteristics, including energy storage, return, [8–11] and/or dissipation [31–33]. We propose a more encompassing approach in designing ankle-foot devices, in which we examine the summed effect of how a group of structures act together during locomotion.

When all biological foot and ankle structures are combined, a recent study in walking found that the net effect of these structures resemble an energy neutral system producing near equal magnitudes of negative and positive work [34]. While the ankle plantar flexor muscle-tendon structures generate most of the positive work within the lower limb [1, 12, 34], foot structures dissipate energy, due to the heel pad [31–33] and the metatarsophalangeal joint [34–37]. In other words, the combined foot-ankle behavior can be analogous to a passive spring that stores and then returns energy (i.e., zero net work). This knowledge of the functions of biological structures could allow versatility in the design of wearable devices: the spring-like behavior of the biological foot-ankle system could be replicated, in theory, via elastic unpowered devices that store and return energy, or the function could be emulated via powered devices that can be actively controlled.

A generalized model that can parameterize the overall functions of the combined foot-ankle system is needed to further facilitate foot and ankle device designs and their customization. One important parameter will be the way in which the ground reaction force, or the location of the center-of-pressure, displaces during stance. It has been shown that the biological foot-ankle system conforms to a rocker-like shape during stance in walking, when the center-of-pressure displacement is viewed within the shank's coordinate system [38–46]. Quantifying or parameterizing this 'roll-over shape' can be informative for understanding the overall behavior of the biological foot and ankle, and has also inspired wearable devices to preserve the biological 'roll-over shape' [41]. One example of recreating this 'roll-over shape' is using a solid ankle boot with a rocker bottom curvature [43]. In this example, the 'roll-over shape' is fixed and rigid, and effectively cannot perform mechanical work. The biological foot and ankle, in contrast, achieves its 'roll-over shape' through the combined effects of ankle joint and toe joint rotations, and plantar surface deformations of the foot [38]. Thus, device designs that mimic 'roll-over shape' may not replicate the mechanical work profiles of the biological foot and ankle. Incorporating forces, displacement and work profiles of the biological ankle and foot in a generalized model will lead to enhanced kinematic and work profiles of customized ankle and foot devices.

The purpose of this study was two fold. First, we aimed to quantify the combined force, displacement, and work of all structures distal to the shank (i.e., foot and ankle) during normal walking. Second, we tested the hypothesis that walking speed, body height, and mass are strong predictors for the individual variability of force, displacement, and work measures. This knowledge would facilitate creation of a simple data-driven, regression-based model that could predict idealized force, displacement, and work measures (distal to the shank) that may be used to customize unpowered wearable foot-ankle devices, such as prostheses and exoskeletons.

Methods

Experimental protocol

Eleven healthy subjects (6 females, 5 males, ages 24.2 ± 2.9 yrs, height 1.72 ± 0.08m, and body mass 75.3 ± 21.8 kg) participated in a fully-instrumented gait analysis. The subjects were screened for any musculoskeletal disorders, and gave written informed consent approved by the IRB at the University of Delaware. Kinematic data (120 Hz) were collected using a six camera-based motion capturing system (Eagle Cameras, Motion Analysis Corp., Santa Rosa, CA), and kinetic data (360 Hz) were collected from a strain gauge force platform (Model OR6-7-2000, 46.4cm x 50.8 cm, AMTI, Watertown, MA). A 6 degrees-of-freedom marker-set [47] was used to estimate lower extremity movement during walking. The subjects walked barefoot at four walking velocities: 0.4, 0.6, 0.8 and 1.0 statures/second (0.69 ± 0.03, 1.03 ± 0.05, 1.38 ± 0.06 and 1.72 ± 0.08 m/s), verified by two photocell beams located approximately 3.0 meters apart. Trials were accepted for analysis if the subject's actual velocity was within ± 0.02 statures/second of the targeted velocity, and if the subjects' entire right foot was observed to contact a single force platform. All data were processed and analyzed using Visual3D software (C-Motion Inc., Germantown, MD). A second-order low-pass Butterworth filter (6Hz for kinematic data, and 25Hz for kinetic data) was applied to the raw data.

Force and displacement distal to the shank

When center-of-pressure (COP) displacement trajectory (i.e., locations of ground reaction force (GRF) application during stance) is transformed from the laboratory coordinate system to the shank's coordinate system (SCS), the COP displacement profile characterizes the 'effective shape' or the 'net deformation' of the ankle and foot structures [38, 41]. Using these concepts, we transformed both the GRF and COP data into the SCS to characterize the force and displacement distal to the shank, respectively (Fig 1). We established the SCS such that the X-axis defined the medial-lateral (M/L) axis, Y-axis defines the anterior-posterior (A/P) axis, the Z-axis defined the superior-inferior (S/I) axis, and the origin was represented by the ankle joint center. Altogether, these kinematic and kinetic data represented the force and displacement profiles of the ankle-foot structures.

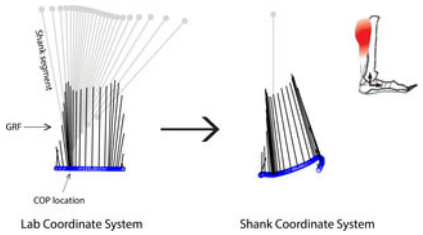

Fig 1. Coordinate transformation.
Both the ground reaction force (GRF) and center of pressure (COP) data were transformed from the lab coordinate system into the shank coordinate system (SCS). This analysis characterized the force and displacement distal to the shank, respectively.
https://doi.org/10.1371/journal.pone.0218047.g001

Power distal to the shank

We quantified the total mechanical power produced by all structures distal to the shank, using a unified deformable segment analysis [48]. This technique synthesizes the GRF and COP displacement relative to the shank, and captures the summed contributions of the ankle and foot structures [48]. Specifically, the COP velocity, or the 'distal velocity' ($\overrightarrow{v_d}$), was quantified (Eq 1) by accounting for the center-of-mass (COM) translational velocity ($\overrightarrow{v_{cm}}$) and segment rotational velocity ($\overrightarrow{\omega_s}$) of the shank, and movement of the COP displacement relative to shank (i.e., the vector from shank COM to COP [$\overrightarrow{r_{COP}}$]).

$$\overrightarrow{v_d} = \overrightarrow{v_{cm}} + (\overrightarrow{\omega_s} \times \overrightarrow{r_{cop}}) \quad (1)$$

The term 'distal' here is used to signify the contributions of all structures distal to the shank, as estimates of $\overrightarrow{v_d}$ can be influenced by ankle and/or foot mechanics. The estimate of $\overrightarrow{r_{COP}}$, notably, is analogous to the COP displacement in the SCS (as defined previously). Then, the power of all structures distal to the shank (P) was quantified (Eq 2) by the summation of the dot product of GRF and $\overrightarrow{v_d}$ and the dot product of force plate free moment ($\overrightarrow{M_{free}}$ – which is the moment about the vertical axis of the laboratory coordinate system) and $\overrightarrow{\omega_s}$.

$$P = \overrightarrow{GRF} \cdot \overrightarrow{v_d} + \overrightarrow{M_{free}} \cdot \overrightarrow{\omega_s} \quad (2)$$

Data analyses

The total COP displacement and the GRF in both the superior-inferior and anterior-posterior directions in the SCS were analyzed. Both of these values were calculated during stance phase, from heel strike to toe-off, with a minimum 20 N vertical GRF threshold. The total excursion of COP displacement in the anterior-posterior axis was determined from the difference between the minimum and maximum COP values. The total excursion of COP displacement in the superior-inferior axis was analyzed by subtracting the maximum COP value from the initial value at heel strike. The GRF peak in the superior-inferior direction was the second peak (during late stance), and the GRF peak in the anterior-posterior direction was the minimum GRF value in the anterior-posterior axis. The positive and negative work distal to the shank was determined by separately integrating the positive and negative power values over time, respectively, using MATLAB (MathWorks Inc., Natick, MA, USA). Net work was the sum of positive and negative work measures.

Statistical analysis

A linear mixed-model ANOVA was used to determine the effects of body height, body mass and speed on the outcome variables (COP displacement, GRF peaks, positive work, negative work, and net work). The analysis was a mixed-model, four-factor ANOVA (random effect: subject; fixed effects: speeds, body height and body mass). All four factors were initially entered into the model, and stepwise elimination was used to eliminate the least significant variables until only the significant terms were left ($p<0.05$). The remaining significant variables were included in the predictor equation for the outcome variables. The coefficients for these variables, as well as the R^2 value for the equation was reported. This analysis was done for each outcome variable (MATLAB; The MathWorks Inc., Natick, MA, USA and IBM SPSS Statistics, IBM, Armonk, NY, USA).

Results

Displacement

The COP in the SCS primarily displaced in the anterior direction during stance (Fig 2A). The total COP displacement in the anterior-posterior direction was 20.33 ± 1.68, 20.43 ± 1.45, 20.64 ± 1.56, and 20.41 ± 1.70 cm for each increasing speed (0.4, 0.6, 0.8, and 1.0 statures/s), respectively. According to the mixed model ANOVA, body height ($p = 0.003$) was a significant predictor of total displacement in the anterior-posterior direction (adjusted $R^2 = 0.76$). Body mass and speed had a non-significant effect on A/P displacement, and thus weren't included in the model. The model predicted the following equation: (Eq 3)

$$Displacement\ A/P\ (cm) = -1.80 + 0.13 * Height\ (cm) \quad (3)$$

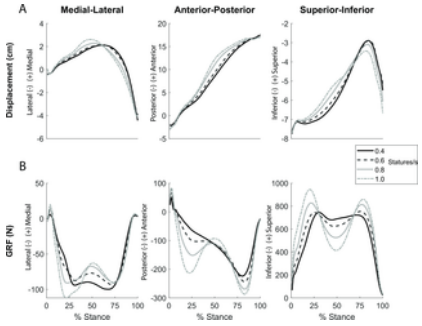

Fig 2.

Center-of-pressure displacement (a) and ground reaction force (b) time series in the shank coordinate system. The different lines represent the 4 speeds (solid line = 0.4 statures/s, dashed line = 0.6 statures/s, dotted line = 0.8 statures/s, and dash dot line = 1.0 statures/s).

https://doi.org/10.1371/journal.pone.0218047.g002

The COP displaced in the superior direction as the ankle dorsiflexed, and the COP displaced in the inferior direction as the ankle plantarflexed (Fig 2A). The total COP displacement in the superior direction was 4.80 ± 0.69, 4.93 ± 1.00, 4.52 ± 1.08, and 4.39 ± 0.91 cm for each speed (0.4, 0.6, 0.8, and 1.0 statures/s), respectively. The mixed model ANOVA determined that body height ($p = 0.004$) and speed ($p = 0.0233$) were significant predictors of total displacement in the superior-inferior direction (adjusted $R^2 = 0.71$). Body mass had a non-significant effect and was therefore removed from the model. The resulting equation was: (Eq 4)

$$Displacement\ S/I\ (cm) = -7.72 - 0.48 * Speed\ (m/s) + 0.08 * Height\ (cm) \quad (4)$$

Force.

The ground reaction force in the SCS anterior-posterior axis was directed in the posterior direction for almost the entirety of stance, primarily because the shank predominately rotated in the forward direction around the medial-lateral axis during stance. The ground reaction force peak in the anterior-posterior (A/P) direction was -225.32 ± 52.86, -245.00 ± 56.24, -270.66 ± 62.16, and -292.03 ± 76.09 N for each increasing speeds (0.4, 0.6, 0.8, and 1.0 statures/s), respectively. Based on the mixed models ANOVA, body mass ($p<0.001$) and speed ($p<0.001$) were significant predictors of peak force in the anterior-posterior direction (adjusted $R^2 = 0.93$). Body height had a non-significant effect on A/P peak force and was therefore removed from the model. The model equation became: (Eq 5)

$$A/P\ Peak\ Force\ (N) = -14.83 - 66.50 * Speed\ (m/s) - 2.17 * Mass\ (kg) \quad (5)$$

The overall pattern of the force in the superior-inferior axis was similar to the vertical GRF in the lab coordinate system [49] in that the force showed two distinct peaks during stance (Fig 2B). The vertical GRF peaks during late stance for each increasing speed were 728.44 ± 209.70, 758.16 ± 219.31, 815.60 ± 239.31, and 861.37 ± 272.52 N respectively. Body mass ($p<0.001$) and speed ($p<0.001$) were significant predictors of peak force in the superior-inferior direction (adjusted $R^2 = 0.98$). Body height had a non-significant effect on S/I peak force and was therefore removed from the model. The resulting model equation is: (Eq 6)

$$S/I\ Peak\ Force\ (N) = -165.58 + 134.77 * Speed\ (m/s) + 10.54 * Mass\ (kg) \quad (6)$$

Power and work

During the first ~75% of stance, the structures distal to the shank (i.e., foot-ankle) produced negative power, whereas during the last ~25% of stance, the structures produced positive power (Fig 3). There was 9.92 ± 4.49, 10.46 ± 3.30, 13.14 ± 4.57, and 16.19 ± 5.68 J of positive work produced for the speed conditions of 0.4, 0.6, 0.8 and 1.0 statures/s, respectively (Fig 4).

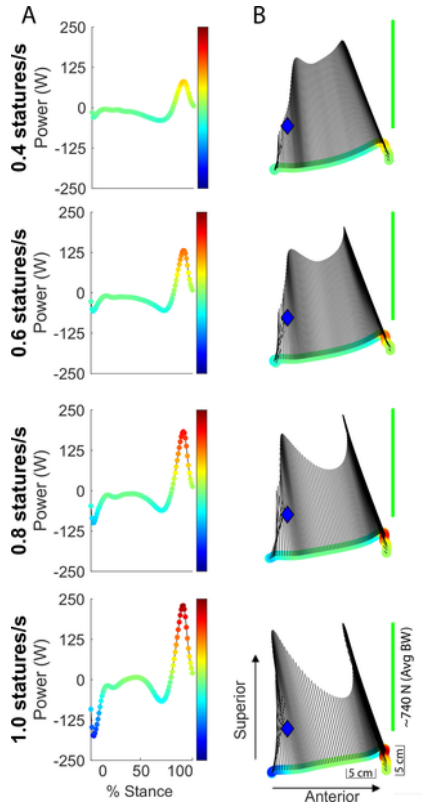

Fig 3. Displacement, force and power distal to the shank.
(a) Average mechanical power distal to the shank during stance phase (N = 11). The colors correspond to the intensity of the instantaneous power. During the first ~75% of stance, the structures distal to the shank (i.e., foot-ankle) produced negative power, whereas during the last ~25% of stance, the structures produced positive power. (b) Displacement, force and power distal to the shank during stance phase. The colored circles indicate displacement of the COP in the shank coordinate system (SCS), and the colors of the circles represent power intensity at each point in stance. Black lines represent the ground reaction force in the SCS, in which the length of the vector denotes the magnitude of the force. Blue diamond represents the location of the ankle joint center in the SCS. The length of the green line represents the magnitude of the average body weight (~740 N).
https://doi.org/10.1371/journal.pone.0218047.g003

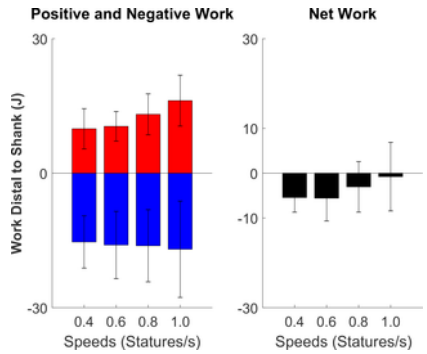

Fig 4. Average mechanical work distal to the shank during stance phase (N = 11).
The magnitude of negative work (red) is slightly greater than positive work (blue), resulting in slight net negative work (black). The magnitude of positive work and net work increased with an increase in speed ($p<0.001$ and $p = 0.0024$), but not negative work ($p = 0.1758$).
https://doi.org/10.1371/journal.pone.0218047.g004

The mixed model ANOVA revealed that body mass ($p<0.001$) and speed ($p<0.001$) were significant predictors of positive work (adjusted $R^2 = 0.86$). Body height had a non-significant effect on positive work and was removed from the model. The resulting model equation was (Eq 7):

$$Positive\ Work\ (J) = -7.61 + 6.23 * Speed\ (m/s) + 0.17 * Mass\ (kg) \quad (7)$$

The amount of negative work for each speed condition was -15.34 ± 5.83, -16.02 ± 7.50, -16.18 ± 8.05, -16.96 ± 10.74 J, respectively. These structures produced slightly greater magnitude of negative work than positive, resulting in slight net negative work (Fig 4).

Mass ($p<0.001$) was found to be a significant predictor of negative work (adjusted $R^2 = 0.90$). Body height and speed had a non-significant effect on negative work and was removed from the model. The resulting model equation for negative work was (Eq 8):

$$Negative\ Work\ (J) = 9.68 - 0.34 * Mass\ (kg) \quad (8)$$

The amount of net work produced for each speed condition was -5.42 ± 3.27, -5.56 ± 5.09, -3.05 ± 5.63, and -0.77 ± 7.65 J. Body mass ($p<0.001$) and speed ($p = 0.0023$) were found to be significant predictors of net work as well (adjusted $R^2 = 0.62$). Body height had a non-significant effect on net work and was removed from the model. The resulting model equation for net work was (Eq 9):

$$Net\ Work\ (J) = 3.83 + 4.61 * Speed\ (m/s) - 0.17 * Mass\ (kg) \quad (9)$$

Discussion

The purpose of this study was to quantify the total force, displacement, and work of all structures distal to the shank in normal walking. Quantifying the force and displacement aids in determining how the biological foot and ankle structures react to the dynamic loads, as well as determining the mechanical work performed by these structures. The distal to shank peak forces, total displacement, and work profiles can be used to create a data-driven model to help customize wearable foot-ankle devices. Our hypothesis was partially supported in that the subject's speed, body height and mass did predict individual variability of peak force, total displacement and work. However, not all of the variables predicted force, displacement, and work.

In previous studies of the 'roll-over shape,' it was found that the COP displacement conforms to a circular shape from heel strike to opposite foot contact [38, 40–46]. Furthermore, this roll-over shape is influenced by the subject's height and is unaffected by walking speed [38]. Our results are in partial agreement in that body height significantly predicted total COP displacement in both the superior-inferior and the anterior-posterior axes. However, we found that speed had an effect on COP displacement in the superior-inferior axes, but not the anterior-posterior axes. In this study, we analyzed each axes of the COP displacement separately, instead of looking at the radii of the curvature [38, 40–42, 45], which could have led to the differing results. We quantified the two axes separately so that we could relate the forces that would cause the displacement along each axes.

By analyzing the force and work, in conjunction with the center-of-pressure displacement, our analyses revealed an emergent property of human foot and ankle function that is analogous to a passive system. In agreement with prior studies [34], the foot and ankle performed net work that did not exceed zero (or was not positive) across various walking speeds, with the amount of negative net work increasing with slower walking speeds. During the slower walking speeds of 0.4 and 0.6 statures/s, the net work was 35.35% and 34.71% of the total negative work, respectively, suggesting that the foot and ankle structures behaved like a spring-damper system. However, as the speed increased to normal walking speeds of 0.8 to 1.0 statures/s, the net work became slightly negative and approaches near zero, while amounting to a much smaller percentage of the total negative work (18.84% and 4.51%). This indicates that the mechanical work production was similar to an ideal spring. Moreover, the spring-like behavior was further evident from the force and displacement profiles along the longitudinal axis of the shank. During the first phase, the COP displaced in the superior direction in the presence of a superior-directed force through most of stance. This may be analogous to a spring being compressed longitudinally, and coincided with the foot-ankle structures performing negative work (Fig 3). During terminal stance, the COP displaced in the inferior direction in the presence of a superior-directed force. This can be compared to a spring recoiling after being compressed, which coincided with the foot-ankle structures performing positive work.

Spring-like analogies of biological limbs, similar to what we found for the foot-ankle system, are ubiquitous in human locomotion studies. For example, the spring-mass model has been used to characterize the center-of-mass movement during the stance phase of running [50–53]. A torsional spring model has been used to describe the moment-angle relationship of the human ankle during stance phase of walking [39, 54–57]. An important characteristic of biological springs is the stiffness (or 'quasi-stiffness'), as measured by the ratio of the peak force and displacement of the leg during running [51, 58–60], or by the ratio of the ankle joint moment and angular displacement during walking [39, 54, 55, 57, 61]. In line with these concepts, we quantified the longitudinal stiffness of the distal-to-shank structures, by computing the ratio of the peak force and total displacement (in the shank's coordinate system). We found that the longitudinal stiffness increased with faster speed ($p = 0.002$), where the stiffness across the four speeds (0.4, 0.6, 0.8, and 1.0 statures/s) was: 153.48 ± 43.81, 156.22 ± 40.31, 187.27 ± 58.52, and 200.71 ± 58.83 N/cm. Our findings support the idea that humans can modulate stiffness of the lower extremity structures across a wide range of locomotor tasks, similar to how the entire leg can modulate stiffness when running on various surfaces [58], or how the ankle joint can modulate stiffness when walking faster [57, 61] or with added mass [57].

Near zero net work done by the human foot and ankle structures may suggest that, in theory, an unpowered device could emulate biological function, either as devices that work with the underlying anatomy (i.e., exoskeletons or orthoses) or replace the structures (i.e., prostheses). In recent years, advancement in unpowered device designs have shown great promise in either augmenting and/or restoring normal walking. A spring-loaded ankle exoskeleton, for example, could reduce metabolic cost of walking in healthy adults [62]. An unpowered prosthesis that harvests collision energy during heel strike could enhance push-off in individuals with limb amputation [63]. Notably, the performance of unpowered devices appear to be largely affected by the selection of key design parameters, such as stiffness. A device that is not too stiff, or too compliant, appears to be favorable for maximizing gait outcomes, as there are mechanical and energetic consequences of using a non-ideal stiffness [64–69]. Furthermore, another feature that may

be important for unpowered devices is the ability to change its stiffness depending on the walking task [70]. As our study, and other studies have found [57, 58, 61], the biological limbs have an inherent ability to modulate joint/limb stiffness based on the demands of locomotion. As such, a device that incorporates micro-motors to alter the stiffness characteristics [70, 71] may be a viable solution to replicate salient features of the biological foot and ankle system.

We developed a regression-based model of the biological foot and ankle mechanics (Table 1), and we envision that this model may be valuable for future design and customization of wearable devices. Most notably, we found that the subject-to-subject variability in peak force, total displacement, and work were well accounted for by three simple factors: the individuals' body height, mass, and walking speed. This knowledge could then be translated into optimizing device characteristics for an individual user by customizing appropriate stiffness, shape, and/or damping (Fig 5). For example, for an individual who is 74.5 kg and 184 cm tall, with a desired walking speed at 1.3 m/s, our regression-based model would predict the following: total A/P displacement of 22.12 cm, total S/I displacement of 6.38 cm, A/P peak force of 262.95 N, S/I peak force of 794.85 N, positive work of 13.15 J, and negative work of -15.85 J. These parameters would enable a bio-inspired device to be designed that would replicate the function of the biological structures.

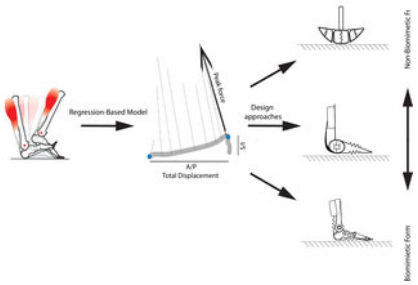

Fig 5. Data-driven regression model of the human foot and ankle function during walking.
In particular, this model can predict an individual's peak force and total displacement along the axes of the shank, as well as positive, negative and net work, based on body height, body mass and speed. This information may be translated into the design of prostheses, orthoses, or exoskeletons that attempt to emulate biological functions with a variety of designs, including both biomimetic and non-biomimetic approaches.
https://doi.org/10.1371/journal.pone.0218047.g005

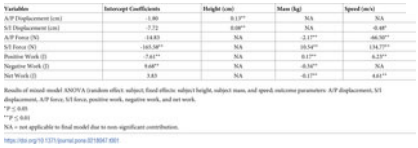

Table 1. Results of mixed-model ANOVA.
https://doi.org/10.1371/journal.pone.0218047.t001

There are some limitations of our model predictions. First, there are other mechanical (e.g., foot anthropometrics, muscle size) and neural (e.g., muscle activation) factors that could influence the peak force, total displacement, and work measures. Second, it is currently unclear how generalizable our model predictions are, since we did not test the accuracy of the model when applied to new individuals, either other healthy adults or persons with gait-related impairments. However, the advantage of our regression-based model is that it does not require biomechanics or gait-based data, and thus may offer a valuable 'initial approximation' towards a subject-specific device prescription. Our model then could be used in conjunction with existing ankle-foot devices that allow fine-adjustments in mechanical characteristics, such as prototypes that contain interchangeable components [62, 64, 65, 69] or through rapid-prototyping or 3-D printing technology [72–75].

By examining mechanics distal to the shank, designs of future foot and ankle devices need not be constrained to mimic biological form (Fig 5). While biomimicry has been central to many foot-ankle devices [28, 62, 76, 77], our generalized model of biological foot and ankle function is not restricted to structures that have anatomical resemblance, such as devices that have an ankle articulation of foot skeleton-like segments. In theory, replicating the 'distal to shank' force, displacement, and work profiles could arise from devices that take on non-biomimetic form. Such non-biomimetic devices are existent in robotic legs inspired from animals [78–81] and in many prosthetic ankle-foot devices that do not have true joint articulations [82–86], for example, running-specific prostheses that emulate spring-like behavior the human leg [83–86]. Our data-driven model may then promote versatility and flexibility in future designs that attempt to replicate biological function via biomimetic and/or non-biomimetic form.

Conclusion

By examining the force, displacement, and work output from structures distal to the shank, we gained novel insights regarding human foot and ankle functions during walking. In particular, the foot and ankle system is analogous to an ideal spring that compresses and recoils along the longitudinal axis of the shank, performing near zero or negative net work across a range of

walking speeds. The subject-to-subject variability in peak force, total displacement and work are predicted by a combination of body mass, body height and walking speed. These findings can create a database of normal gait that can inform the design and customization of unpowered foot-ankle device (e.g. prostheses, exoskeletons) that can emulate biological functions during walking.

Supporting information

S1 Table. Subject specific data and average data.
Subject specific data contributing to the mixed-model ANOVA are included. The data also include average data contributing to the center-of-pressure displacement and ground reaction force, time series in the shank coordinate system, as well as the average mechanical power and work distal to the shank during the stance phase.
https://doi.org/10.1371/journal.pone.0218047.s001
(XLSX)

References

1. DeVita P, Helseth J, Hortobagyi T. Muscles do more positive than negative work in human locomotion. J Exp Biol. 2007 OCT 1;210(19):3361–73.
View Article • Google Scholar

2. Winter DA. Energy Generation and Absorption at the Ankle and Knee during Fast, Natural, and Slow Cadences. Clin Orthop. 1983(175):147–54. pmid:6839580
View Article • PubMed/NCBI • Google Scholar

3. Cavagna GA, Kaneko M. Mechanical Work and Efficiency in Level Walking and Running. J Physiol -London. 1977;268(2):467–81. pmid:874922
View Article • PubMed/NCBI • Google Scholar

4. Elftman H. The function of muscles in locomotion. Am J Physiol. 1939 FEB;125(2):357–66.
View Article • Google Scholar

5. Neptune RR, Kautz SA, Zajac FE. Contributions of the individual ankle plantar flexors to support, forward progression and swing initiation during walking. J Biomech. 2001 NOV;34(11):1387–98. pmid:11672713
View Article • PubMed/NCBI • Google Scholar

6. Zelik KE, Adamczyk PG. A unified perspective on ankle push-off in human walking. J Exp Biol. 2016 DEC 1;219(23):3676–83.
View Article • Google Scholar

7. Lichtwark GA, Wilson AM. Interactions between the human gastrocnemius muscle and the Achilles tendon during incline, level and decline locomotion. J Exp Biol. 2006 NOV 1;209(21):4379–88.
View Article • Google Scholar

8. Ker RF, Bennett MB, Bibby SR, Kester RC, Alexander RM. The Spring in the Arch of the Human Foot. Nature. 1987 January 8,;325(6100):147–9.
View Article • Google Scholar

9. Stearne SM, McDonald KA, Alderson JA, North I, Oxnard CE, Rubenson J. The Foot's Arch and the Energetics of Human Locomotion. Sci Rep. 2016 JAN 19;6:19403. pmid:26783259
View Article • PubMed/NCBI • Google Scholar

10. Lichtwark GA, Bougoulias K, Wilson AM. Muscle fascicle and series elastic element length changes along the length of the human gastrocnemius during walking and running. J Biomech. 2007;40(1):157–64. pmid:16364330
View Article • PubMed/NCBI • Google Scholar

11. Erdemir A, Hamel AJ, Fauth AR, Piazza SJ, Sharkey NA. Dynamic loading of the plantar aponeurosis in walking. J Bone Joint Surg -Am Vol. 2004 MAR;86A(3):546–52.
View Article • Google Scholar

12. Farris DJ, Sawicki GS. The mechanics and energetics of human walking and running: a joint level perspective. J R Soc Interface. 2012 JAN 7;9(66):110–8. pmid:21613286
View Article • PubMed/NCBI • Google Scholar

13. Fukunaga T, Kubo K, Kawakami Y, Fukashiro S, Kanehisa H, Maganaris CN. In vivo behaviour of human muscle tendon during walking. Proc R Soc B-Biol Sci. 2001 FEB 7;268(1464):229–33.
View Article • Google Scholar

14. Fukunaga T, Kawakami Y, Kubo K, Kanehisa H. Muscle and tendon interaction during human movements. Exerc Sport Sci Rev. 2002 JUL;30(3):106–10. pmid:12150568
View Article • PubMed/NCBI • Google Scholar

15. Sawicki GS, Lewis CL, Ferris DP. It Pays to Have a Spring in Your Step. Exerc Sport Sci Rev. 2009 JUL;37(3):130–8. pmid:19550204
View Article • PubMed/NCBI • Google Scholar

16. Ishikawa M, Komi PV, Grey MJ, Lepola V, Bruggemann GP. Muscle-tendon interaction and elastic energy usage in human walking. J Appl Physiol. 2005 AUG;99(2):603–8. pmid:15845776
View Article • PubMed/NCBI • Google Scholar

17. Roberts TJ, Azizi E. Flexible mechanisms: the diverse roles of biological springs in vertebrate movement. J Exp Biol. 2011 FEB;214(3):353–61.
View Article • Google Scholar

18. Huang TP, Shorter KA, Adamczyk PG, Kuo AD. Mechanical and energetic consequences of reduced ankle plantar-flexion in human walking. J Exp Biol. 2015 NOV;218(22):3541–50.
View Article • Google Scholar

19. Guan X, Kuai S, Ji L, Wang R, Ji R. Trunk muscle activity patterns and motion patterns of patients with motor complete spinal cord injury at T8 and T10 walking with different un-powered exoskeletons. J Spinal Cord Med. 2017;40(4):463–70. pmid:28514926
View Article • PubMed/NCBI • Google Scholar

20. Boes MK, Bollaert RE, Kesler RM, Learmonth YC, Islam M, Petrucci MN, et al. Six-Minute Walk Test Performance in Persons With Multiple Sclerosis While Using Passive or Powered Ankle-Foot Orthoses. Arch Phys Med Rehabil. 2018 MAR;99(3):484–90. pmid:28778829
View Article • PubMed/NCBI • Google Scholar

21. Arch ES, Stanhope SJ, Higginson JS. Passive-dynamic ankle–foot orthosis replicates soleus but not gastrocnemius muscle function during stance in gait: Insights for orthosis prescription. Prosthetics and Orthotics International. 2016 Oct;40(5):606–16. pmid:26209424
View Article • PubMed/NCBI • Google Scholar

22. Arch ES, Stanhope SJ. Passive-Dynamic Ankle-Foot Orthoses Substitute for Ankle Strength While Causing Adaptive Gait Strategies: A Feasibility Study. Ann Biomed Eng. 2015 FEB;43(2):442–50. pmid:25023660
View Article • PubMed/NCBI • Google Scholar

23. Koller JR, Remy CD, Ferris DP. Biomechanics and energetics of walking in powered ankle exoskeletons using myoelectric control versus mechanically intrinsic control. J NeuroEng Rehabil. 2018 MAY 25;15:42. pmid:29801451
View Article • PubMed/NCBI • Google Scholar

24. Takahashi KZ, Lewek MD, Sawicki GS. A neuromechanics-based powered ankle exoskeleton to assist walking post-stroke: a feasibility study. Journal of neuroengineering and rehabilitation. 2015 Feb 25,;12(1):23.
View Article • Google Scholar

25. Wu C, Mao H, Hu J, Wang T, Tsai Y, Hsu W. The effects of gait training using powered lower limb exoskeleton robot on individuals with complete spinal cord injury. J NeuroEng Rehabil. 2018 MAR 5;15:14. pmid:29506530
View Article • PubMed/NCBI • Google Scholar

26. Galle S, Malcolm P, Derave W, De Clercq D. Enhancing performance during inclined loaded walking with a powered ankle-foot exoskeleton. Eur J Appl Physiol. 2014 NOV;114(11):2341–51. pmid:25064193
View Article • PubMed/NCBI • Google Scholar

27. Awad LN, Bae J, O'Donnell K, De Rossi, Stefano M M, Hendron K, Sloot LH, et al. A soft robotic exosuit improves walking in patients after stroke. Science translational medicine. 2017 Jul 26,;9(400):eaai9084. pmid:28747517
View Article • PubMed/NCBI • Google Scholar

28. Herr HM, Grabowski AM. Bionic ankle-foot prosthesis normalizes walking gait for persons with leg amputation. Proc R Soc B-Biol Sci. 2012 FEB 7;279(1728):457–64.
View Article • Google Scholar

29. Malcolm P, Quesada RE, Caputo JM, Collins SH. The influence of push-off timing in a robotic ankle-foot prosthesis on the energetics and mechanics of walking. J NeuroEng Rehabil. 2015 FEB 22;12:21. pmid:25889201
View Article • PubMed/NCBI • Google Scholar

30. Quesada RE, Caputo JM, Collins SH. Increasing ankle push-off work with a powered prosthesis does not necessarily reduce metabolic rate for transtibial amputees. J Biomech. 2016 OCT 3;49(14):3452–9. pmid:27702444
View Article • PubMed/NCBI • Google Scholar

31. Gefen A, Megido-Ravid M, Itzchak Y. In vivo biomechanical behavior of the human heel pad during the stance phase of gait. J Biomech. 2001 DEC;34(12):1661–5. pmid:11716870
View Article • PubMed/NCBI • Google Scholar

32. Aerts P, Ker RF, Declercq D, Ilsley DW, Alexander RM. The Mechanical-Properties of the Human Heel Pad—a Paradox Resolved. J Biomech. 1995 NOV;28(11):1299–308. pmid:8522543
View Article • PubMed/NCBI • Google Scholar

33. Wearing SC, Hooper SL, Dubois P, Smeathers JE, Dietze A. Force-Deformation Properties of the Human Heel Pad during Barefoot Walking. Med Sci Sports Exerc. 2014 AUG;46(8):1588–94. pmid:24504425
View Article • PubMed/NCBI • Google Scholar

34. Takahashi KZ, Worster K, Bruening DA. Energy neutral: the human foot and ankle subsections combine to produce near zero net mechanical work during walking. Sci Rep. 2017 NOV 13;7:15404. pmid:29133920
View Article • PubMed/NCBI • Google Scholar

35. Takahashi KZ, Stanhope SJ. Mechanical energy profiles of the combined ankle-foot system in normal gait: Insights for prosthetic designs. Gait Posture. 2013 SEP;38(4):818–23. pmid:23628408
View Article • PubMed/NCBI • Google Scholar

36. Stefanyshyn DJ, Nigg BM. Mechanical energy contribution of the metatarsophalangeal joint to running and sprinting. J Biomech. 1997;30(11–12):1081–5. pmid:9456374
View Article • PubMed/NCBI • Google Scholar

37. Willwacher S, Koenig M, Potthast W, Brueggemann G. Does Specific Footwear Facilitate Energy Storage and Return at the Metatarsophalangeal Joint in Running? J Appl Biomech. 2013 OCT;29(5):583–92. pmid:24203172
View Article • PubMed/NCBI • Google Scholar

38. Hansen AH, Childress DS, Knox EH. Roll-over shapes of human locomotor systems: effects of walking speed. Clin Biomech. 2004 MAY;19(4):407–14.
View Article • Google Scholar

39. Hansen AH, Childress DS, Miff SC, Gard SA, Mesplay KP. The human ankle during walking: implications for design of biomimetic ankle prostheses. J Biomech. 2004;37(10):1467–74. pmid:15336920
View Article • PubMed/NCBI • Google Scholar

40. Hansen AH, Childress DS. Effects of adding weight to the torso on roll-over characteristics of walking. J Rehabil Res Dev. 2005;42(3):381–90. pmid:16187250
View Article • PubMed/NCBI • Google Scholar

41. Hansen AH, Childress DS. Investigations of roll-over shape: implications for design, alignment, and evaluation of ankle-foot prostheses and orthoses. Disabil Rehabil. 2010;32(26):2201–9. pmid:20626257
View Article • PubMed/NCBI • Google Scholar

42. Wang CC, Hansen AH. Response of able-bodied persons to changes in shoe rocker radius during walking: Changes in ankle kinematics to maintain a consistent roll-over shape. J Biomech. 2010 AUG 26;43(12):2288–93. pmid:20483413
View Article • PubMed/NCBI • Google Scholar

43. Adamczyk PG, Collins SH, Kuo AD. The advantages of a rolling foot in human walking. J Exp Biol. 2006 OCT 15;209(20):3953–63.
View Article • Google Scholar

44. Hansen AH, Childress DS. Effects of shoe heel height on biologic rollover characteristics during walking. Journal of rehabilitation research and development. 2004 Jul;41(4):547. pmid:15558383
View Article • PubMed/NCBI • Google Scholar

45. Hansen AH, Childress DS, Miff SC. Roll-over characteristics of human walking on inclined surfaces. Hum Mov Sci. 2004 DEC;23(6):807–21. pmid:15664674
View Article • PubMed/NCBI • Google Scholar

46. Owen E, Fatone S, Hansen A. Effect of walking in footwear with varying heel sole differentials on shank and foot segment kinematics. Prosthet Orthot Int. 2018 AUG;42(4):394–401. pmid:28884616
View Article • PubMed/NCBI • Google Scholar

47. Holden JP, Chou G, Stanhope SJ. Changes in knee joint function over a wide range of walking speeds. Clin Biomech. 1997 SEP;12(6):375–82.
View Article • Google Scholar

48. Takahashi KZ, Kepple TM, Stanhope SJ. A unified deformable (UD) segment model for quantifying total power of anatomical and prosthetic below-knee structures during stance in gait. J Biomech. 2012 OCT 11;45(15):2662–7. pmid:22939292

View Article • PubMed/NCBI • Google Scholar

49. Winter DA. Biomechanics and motor control of human movement. 4. ed. ed. Hoboken, NJ: Wiley; 2009.

50. Lee DV, Isaacs MR, Higgins TE, Biewener AA, McGowan CP. Scaling of the Spring in the Leg during Bouncing Gaits of Mammals. Integr Comp Biol. 2014 DEC;54(6):1099–108. pmid:25305189
View Article • PubMed/NCBI • Google Scholar

51. McMahon TA, Cheng GC. The Mechanics of Running—how does Stiffness Couple with Speed. J Biomech. 1990;23:65–78. pmid:2081746
View Article • PubMed/NCBI • Google Scholar

52. Blickhan R, Full RJ. Similarity in Multilegged Locomotion—Bouncing Like a Monopode. J Comp Physiol A-Sens Neural Behav Physiol. 1993 NOV;173(5):509–17.
View Article • Google Scholar

53. Blickhan R. The Spring Mass Model for Running and Hopping. J Biomech. 1989;22(11–12):1217–27. pmid:2625422
View Article • PubMed/NCBI • Google Scholar

54. Shamaei K, Sawicki GS, Dollar AM. Estimation of Quasi-Stiffness and Propulsive Work of the Human Ankle in the Stance Phase of Walking. PLoS One. 2013 MAR 21;8(3):e59935.
View Article • Google Scholar

55. Crenna P, Frigo C. Dynamics of the ankle joint analyzed through moment–angle loops during human walking: Gender and age effects. Human Movement Science. 2011 Dec;30(6):1185–98. pmid:21669469
View Article • PubMed/NCBI • Google Scholar

56. Frigo C, Crenna P, Jensen LM. Moment-angle relationship at lower limb joints during human walking at different velocities. J Electromyogr Kinesiol. 1996 SEP;6(3):177–90. pmid:20719675
View Article • PubMed/NCBI • Google Scholar

57. Shamaei K, Cenciarini M, Dollar AM. On the Mechanics of the Ankle in the Stance Phase of the Gait IEEE Engineering in Medicine and Biology Society. 2011:8135–40.
View Article • Google Scholar

58. Ferris DP, Louie M, Farley CT. Running in the real world: adjusting leg stiffness for different surfaces. Proc R Soc B-Biol Sci. 1998 JUN 7;265(1400):989–94.
View Article • Google Scholar

59. Blum Y, Lipfert SW, Seyfarth A. Effective leg stiffness in running. J Biomech. 2009 OCT 16;42(14):2400–5. pmid:19647825
View Article • PubMed/NCBI • Google Scholar

60. Arampatzis A, Bruggemann GP, Metzler V. The effect of speed on leg stiffness and joint kinetics in human running. J Biomech. 1999 DEC;32(12):1349–53. pmid:10569714
View Article • PubMed/NCBI • Google Scholar

61. Collins JD, Arch ES, Crenshaw JR, Bernhardt KA, Khosla S, Amin S, et al. Net ankle quasi-stiffness is influenced by walking speed but not age for older adult women. Gait & posture. 2018;62:316.
View Article • Google Scholar

62. Collins SH, Wiggin MB, Sawicki GS. Reducing the energy cost of human walking using an unpowered exoskeleton. Nature. 2015 JUN 11;522(7555).
View Article • Google Scholar

63. Segal AD, Zelik KE, Klute GK, Morgenroth DC, Hahn ME, Orendurff MS, et al. The effects of a controlled energy storage and return prototype prosthetic foot on transtibial amputee ambulation. Human Movement Science. 2012 Aug;31(4):918–31. pmid:22100728
View Article • PubMed/NCBI • Google Scholar

64. Major MJ, Twiste M, Kenney LPJ, Howard D. The effects of prosthetic ankle stiffness on ankle and knee kinematics, prosthetic limb loading, and net metabolic cost of trans-tibial amputee gait. Clin Biomech. 2014 JAN;29(1):98–104.
View Article • Google Scholar

65. Adamczyk PG, Roland M, Hahn ME. Sensitivity of biomechanical outcomes to independent variations of hindfoot and forefoot stiffness in foot prostheses. Human Movement Science. 2017 AUG;54:154–71. pmid:28499159
View Article • PubMed/NCBI • Google Scholar

66. Fey NP, Klute GK, Neptune RR. Altering prosthetic foot stiffness influences foot and muscle function during below-knee amputee walking: A modeling and simulation analysis. J Biomech. 2013 FEB 22;46(4):637–44. pmid:23312827
View Article • PubMed/NCBI • Google Scholar

67. Fey NP, Klute GK, Neptune RR. The influence of energy storage and return foot stiffness on walking mechanics and muscle activity in below-knee amputees. Clin Biomech. 2011 DEC;26(10):1025–32.
View Article • Google Scholar

68. Shell CE, Segal AD, Klute GK, Neptune RR. The effects of prosthetic foot stiffness on transtibial amputee walking mechanics and balance control during turning. Clin Biomech. 2017 NOV;49:56–63.
View Article • Google Scholar

69. Honert EC, Bastas G, Zelik KE. Effect of toe joint stiffness and toe shape on walking biomechanics. Bioinspiration & biomimetics. 2018 Sep 6,.
View Article • Google Scholar

70. Shepherd MK, Rouse EJ. The VSPA Foot: A Quasi-Passive Ankle-Foot Prosthesis With Continuously Variable Stiffness. TNSRE. 2017;25(12):2375–86.
View Article • Google Scholar

71. Glanzer EM, Adamczyk PG. Design and Validation of a Semi-Active Variable Stiffness Foot Prosthesis. IEEE Trans Neural Syst Rehabil Eng. 2018 October 25,:1.
View Article • Google Scholar

72. Schrank ES, Hitch L, Wallace K, Moore R, Stanhope SJ. Assessment of a Virtual Functional Prototyping Process for the Rapid Manufacture of Passive-Dynamic Ankle-Foot Orthoses. J Biomech Eng -Trans ASME. 2013 OCT;135(10):101011.
View Article • Google Scholar

73. Faustini MC, Neptune RR, Crawford RH, Stanhope SJ. Manufacture of passive dynamic ankle-foot orthoses using selective laser sintering. IEEE Trans Biomed Eng. 2008 FEB;55(2):784–90.
View Article • Google Scholar

74. Cha YH, Lee KH, Ryu HJ, Joo IW, Seo A, Kim D, et al. Ankle-Foot Orthosis Made by 3D Printing Technique and Automated Design Software. Appl Bionics Biomech. 2017:9610468. pmid:28827977
View Article • PubMed/NCBI • Google Scholar

75. Harper NG, Russell EM, Wilken JM, Neptune RR. Selective Laser Sintered Versus Carbon Fiber Passive-Dynamic Ankle-Foot Orthoses: A Comparison of Patient Walking Performance. J Biomech Eng -Trans ASME. 2014 SEP;136(9):091001.
View Article • Google Scholar

76. Mooney LM, Lai CH, Rouse EJ. Design and characterization of a biologically inspired quasi-passive prosthetic ankle-foot. United States: IEEE; Aug 2014.

77. Bai X, Ewins D, Crocombe AD, Xu W. Kinematic and biomimetic assessment of a hydraulic ankle/foot in level ground and camber walking. PLoS One. 2017 JUL 13;12(7):e0180836. pmid:28704428
View Article • PubMed/NCBI • Google Scholar

78. Ananthanarayanan A, Azadi M, Kim S. Towards a bio-inspired leg design for high-speed running. Bioinspir Biomim. 2012 DEC;7(4):046005. pmid:22872655
View Article • PubMed/NCBI • Google Scholar

79. Raibert M, Blankespoor K, Nelson G, Playter R. Bigdog, the rough-terrain quadruped robot. P 17 WORLD C INT FED. 2008:10822–5.
View Article • Google Scholar

80. Spenko MJ, Haynes GC, Saunders JA, Cutkosky MR, Rizzi AA, Full RJ, et al. Biologically inspired climbing with a hexapedal robot. J Field Robot. 2008;25(4–5):223–42.
View Article • Google Scholar

81. Lambrecht B, Horchler AD, Quinn RD. A small, insect-inspired robot that runs and jumps. NEW YORK: IEEE; 2005.

82. Versluys R, Beyl P, Van Damme M, Desomer A, Van Ham R, Lefeber D. Prosthetic feet: State-of-the-art review and the importance of mimicking human ankle-foot biomechanics. Disability & Rehabilitation: Assistive Technology. 2009;4(2):65–75.
View Article • Google Scholar

83. Beck ON, Grabowski AM. Athletes with Versus Without Leg Amputations: Different Biomechanics, Similar Running Economy. Exercise and Sport Sciences Reviews. 2018.
View Article • Google Scholar

84. Brown MB, Millard-Stafford ML, Allison AR. Running-Specific Prostheses Permit Energy Cost Similar to Nonamputees. Med Sci Sports Exerc. 2009 MAY;41(5):1080–7. pmid:19346979
View Article • PubMed/NCBI • Google Scholar

85. Weyand PG, Bundle MW, McGowan CP, Grabowski A, Brown MB, Kram R, et al. The fastest runner on artificial legs: different limbs, similar function? J Appl Physiol. 2009 SEP;107(3):903–11. pmid:19541739
View Article • PubMed/NCBI • Google Scholar

86. Willwacher S, Funken J, Heinrich K, Mueller R, Hobara H, Grabowski AM, et al. Elite long jumpers with below the knee prostheses approach the board slower, but take-off more effectively than non-amputee athletes. Sci Rep. 2017 NOV 22;7:16058. pmid:29167568
View Article • PubMed/NCBI • Google Scholar